CAR-MACROPHAGES ACTIVATE ANTI TUMOR T CELLS IN THE ABSENCE OF PHAGOCYTOSIS

Lea Feldmann[1], Amaury Vaysse[2*], Fabrice Lemaître[1*], Béatrice Corre[1*], Ruby Alonso[1], Camille Vaganay[1], Marion V. Guérin[1], Zacarias Garcia[1], Philippe Bousso[1] and Capucine L. Grandjean[1]

[1] Dynamics of Immune Responses Unit, Université Paris Cité, Institut Pasteur, INSERM U1223, Paris, France.
[2] Institut Pasteur, Université Paris Cité, Bioinformatics and Biostatistics Hub, Paris, France
[*] These authors contributed equally to the work.

Correspondence to capucine.grandjean@pasteur.fr

ABSTRACT (207 words)

Macrophages are highly abundant within the tumor microenvironment and serve as an essential bridge between innate and adaptive immune responses. Thus, they have emerged as promising candidates for chimeric antigen receptor (CAR)-based therapeutic strategies. Previous studies demonstrated that adenovirally-transduced CAR-macrophages (CAR-M), used in clinical trials, can perform tumor cell phagocytosis, reshape the tumor microenvironment towards a proinflammatory state, and promote host T cell activation. However, how early interactions between CAR-M and tumor cells shape subsequent T cell effector functions remains poorly understood. Particularly, uncoupling the adenoviral-induced proinflammatory phenotype from CAR-M effector functions remains to be dissected. Here, using phagocytosis-optimized CAR-Ms, we demonstrated that T cells are crucial mediators of CAR-M therapeutic efficacy. Mechanistically, we identify that CAR-M-derived cytokines and chemokines are key drivers of T cell functions while antigen cross presentation appears largely dispensable. Dynamic imaging of CAR-M-tumor cell interactions revealed heterogenous phagocytic abilities, regardless of contact duration. Finally, we show that non-phagocytic interactions can instruct pro-inflammatory macrophage repolarization and subsequent T cell activation. Altogether, these findings define an alternative mode of CAR-M action in which CAR engagement alone, independently of target cell uptake, is sufficient to enhance T cell functions. Our study underscores the importance of non-phagocytic CAR signaling as an additional mechanism for CAR-M effector functions opening new avenues for the design of next generation CAR for macrophage-based therapies.

Significance statement (117 words)

Macrophages are a crucial player of the tumor microenvironment. They have been targeted for therapies, for example by arming them with a chimeric antigen receptor (CAR). CAR-macrophages (CAR-M) are currently in clinical trials, but their precise mechanism of action remains poorly understood. The prevailing model proposes that enhanced phagocytosis by CAR-M leads to T cell activation. Here, using dynamic imaging, we uncover substantial heterogeneity in CAR-M ability to engulf tumor cells. However, we show that CAR engagement albeit lack of tumor engulfment, can produce proinflammatory mediators to activate T cells. Thus, our study recenter CAR signaling, in the absence of tumor engulfment, as a complementary mode of action of CAR-M, opening new strategies for next generation CAR-macrophages.

INTRODUCTION

Macrophages are among the most abundant immune cell populations in solid tumors (1). Although tumor-associated macrophages often acquire immunosuppressive and pro-tumoral functions that facilitate tumor progression, they retain a remarkable degree of functional plasticity (2). In response to appropriate cues, macrophages can adopt a pro-inflammatory state, thereby promoting anti-tumor immunity and contributing to tumor regression in some contexts (3). Through their ability to fine-tune immune responses and bridge innate and adaptive immunity, macrophages act as key regulators of the tumor microenvironment (2). This functional duality has positioned macrophages at the forefront of emerging cancer immunotherapy strategies.

Initial macrophage-targeting therapeutic strategies focused on reducing macrophage abundance in tumors, either by selectively eliminating immunosuppressive populations (4, 5) or by limiting their recruitment, notably through blockade of the colony stimulating factor-1 (CSF-1)-receptor axis (6,7). More recently, the field has expanded to include approaches that actively reprogram macrophages toward a pro-inflammatory phenotype, by stimulating activating cascades (e.g. CD40, toll-like receptor (TLR) agonists) (8, 9). In parallel, antibody-based therapies have sought to enhance macrophage phagocytic activity by disrupting inhibitory axis, with the dual objective of triggering tumor clearance and antigen cross-presentation to T cells *(10–13)*.

Alongside these approaches, a distinct strategy has emerged involving the engineering of macrophages to express chimeric antigen receptors (CAR-M), inspired by the clinical success of CAR-T cell therapies in hematological malignancies (14, 15). CAR-M have now entered early-phase clinical trials, however their mechanisms of action remain incompletely understood (16). Adenovirally-generated CAR-M expressing a CAR composed of the canonical T cell signaling domain CD3ζ, have been shown to mediate tumor cell phagocytosis highlighting redundancy in the signaling cascade of T cells and macrophages (17). These CAR-M acquired a strong pro-inflammatory phenotype associated with enhanced T cell responses mainly driven by the adenoviral transduction approach (18, 19). How this pre-acquired pro-inflammatory CAR-M phenotype can be uncoupled from CAR-driven effector functions remains an unresolved question.

A prevailing model posits that CAR-mediated engulfment of tumor cells drives antitumor immunity not only through direct tumor debulking but also by T cell priming through antigen cross-presentation (15). Under this framework, optimizing CAR-M phagocytic activity is expected to directly enhance T cell activation and therapeutic efficacy. However, whether CAR-M-mediated T cell activation strictly depends on phagocytosis or instead can be driven by alternative CAR-dependent signaling pathways, remains to be addressed.

Here, we demonstrate that CAR-M enhance T cell responses through a dual phagocytic and non-phagocytic mechanism. By combining real-time imaging with functional reporters to simultaneously monitor phagocytosis and CAR signaling, we dissect the early interactions between CAR-M and tumor cells. Surprisingly, despite prolonged contacts, not all CAR-M engulf tumor cells despite CAR signaling, revealing marked functional heterogeneity within the CAR-M population. Using mixed-species bulk RNA sequencing and multiplexed protein analysis, we show that CAR signaling alone, even in the absence of phagocytosis, is sufficient to induce a pro-inflammatory transcriptional program in CAR-M, thereby driving cytokine production and T cell activation. Collectively, these findings identify CAR engagement itself as a key instructive signal that promotes CAR-M pro-inflammatory functions, regardless of phagocytosis, thereby enhancing adaptive immune responses.

RESULTS

Retrovirally-transduced non-polarized CAR-M can mediate tumor control.

In clinical trial, CAR-M therapies rely on adenoviral transduction of a first-generation CAR containing the CD3ζ immunoreceptor tyrosine-based activation motifs (ITAMs), a canonical T cell signaling module that can also activate kinases in macrophages (17). Mechanistic *in vivo* studies have demonstrated that these pro-inflammatory CAR-M engulf tumor cells, repolarize the tumor microenvironment and enhance anti-tumor T cell responses *(18–20)*. In these settings, adenoviral transduction was required for polarizing CAR-M into a pro-inflammatory state, a prerequisite for therapeutic efficacy. Whether CAR-M-mediated crosstalk with T cells extends beyond this specific transduction platform, however, remains unclear.

To explore the antitumoral effect of CAR-M independently of adenoviral interference in macrophage inflammatory status, we relied on the retroviral transduction of a macrophage-specific CAR-construct. This anti-CD19 receptor is composed of the intracellular FcRγ-ITAM and a PI3K recruiting domain. This CAR has been shown previously to improve CAR-mediated phagocytosis (17) (**Fig 1A**). CAR-expressing bone marrow-derived macrophages (BMDM) were generated, and CAR-expression was assessed by surface expression of the human CD34 (hCD34) reporter encoded along the CAR construct via a self-cleaving 2A peptide or by direct CAR detection (**Fig 1B and S1D**). Control macrophages were sham transduced with empty retroviral particles (M^{Empty}).

First, to determine whether retroviral transduction would tune macrophage inflammatory status, we analyzed cytokine and chemokine production over 24 h in supernatants from CAR-M and compared with untransduced macrophages (M^{UTD}), M^{Empty} and macrophages pre-treated with lipopolysaccharide (LPS) as positive control (**Fig. 1C**). As expected, LPS stimulation induced a robust inflammatory response. In contrast, no substantial differences in cytokine secretion were identified between CAR-M, M^{UTD} and M^{Empty} conditions (**Fig. 1D and S2**), suggesting that retroviral transduction did not intrinsically skew macrophages toward a pro-inflammatory state. Thus, CAR-Ms generated from BMDM by retroviral transduction do not constitutively upregulate a pro-inflammatory program at steady state.

We next assessed the capacity of CAR-M to eliminate tumor cells both *in vitro* and *in vivo*, using both hematological and epithelial/mesenchymal tumor models. In a co-culture assay, we first evaluated CAR-M elimination of CD19-expressing tumor cells *in vitro* including Eμ-Myc and ProB tumor B cell lines and CD19-engineered MC38 colon carcinoma and B16_F10 melanoma cells (**Fig. 1E**). Across all tumor models, CAR-M significantly eliminated tumor cells within 48 h compared to control macrophages (**Fig. 1F-G**). Early tumor cell elimination was then evaluated *in vivo* by intraperitoneally injection of solid (MC38) or liquid (ProB) tumor cells into C57BL/6 mice, followed by CAR-M administration (**Fig. 1H**). Analysis within 48 h post-treatment revealed a significant reduction in tumor load in CAR-M-treated mice, consistent with efficient phagocytosis of the tumor cells (**Fig. 1I**). Thus, these results demonstrate that regardless of a pre-acquired pro-inflammatory phenotype, CAR-M rapidly eliminate diverse tumor cell types both *in vitro* and *in vivo*.

CAR-M-derived pro-inflammatory cytokines, upon tumor contacts, enhance T cell activation

Adenovirally-transduced CAR-M have been shown to promote T cell-mediated adaptive immune responses through antigen cross-presentation, thereby contributing to sustained tumor control (18, 20). Thus, we first assessed whether CAR-M in our settings could enhance T cell activation through antigen cross-presentation. To this aim, CAR-M or M^{UTD} were co-cultured with ovalbumin (OVA)-expressing tumor cells for 4 h, similar to previous set-ups of antigen cross-presentation (20). This was followed by extensive washing to remove most tumor cells and the addition of CellTrace Violet (CTV)-labelled naïve OVA-specific $CD8^+$ T cells (OT-I cells) for 48 h (**Fig. 2A**). To assess CAR-M cross-presentation ability independently of direct T cell recognition, we used both wild-type (WT) and β2-microglobulin-deficient (*β2m*$^{-/-}$) tumor cells, preventing MHC-I surface expression (**Fig. S3A**). OT-I cells proliferated in the presence of MHC-I-sufficient tumor cells but failed to divide when MHC-I-deficient tumor cells were used (**Fig. 2B and S3B**). Importantly, CAR-M enhanced T cell proliferation only in the presence of MHC-I-sufficient tumor cells. These results suggest that initial T cell activation is driven by direct recognition of tumor antigens, while CAR-M act to enhance T cell response independently of CAR-M antigen cross-presentation.

We next sought to evaluate whether CAR-M-mediated enhancement of T cell responses could occur in a contact-independent manner by soluble factors. To test this hypothesis, we performed transwell assays in which CAR-M were physically separated from naïve OT-I T cells and tumor cells (**Fig. 2C**). Under these conditions, T cells exposed to CAR-M-derived soluble factors exhibited proliferation and activation. This was significantly increased compared with those exposed to macrophages expressing a non-signaling CAR, lacking intracellular domains, CAR^{CTRL}-M, a phenotype associated to increased T cell numbers (**Fig. 2D-F and S4A**). Functional analyses showed that CAR-M promoted enhanced cytotoxic differentiation, as indicated by increased frequencies of granzyme B-expressing T cells and elevated granzyme B expression levels (**Fig. 2G-I and S4B**). Moreover, they revealed a higher proportion of tumor necrosis factor alpha high ($TNFα^{high}$) T cells in the presence of CAR-M (**Fig. 2J and S4C**). Notably, the T cells exhibited a trend toward a central memory-like phenotype ($CD62L^+$ $CD44^+$), which has been associated with improved tumor control (21) (**Fig. 2K-L**). Together, these results indicate that CAR-M co-cultured with tumor cells release soluble factors that enhance T cell activation.

To define the nature of these mediators, we performed a multiplex assay on supernatants from CAR-M–tumor co-cultures following tumor engagement (**Fig. 2M**). CAR-M and tumor cell co-cultures exhibited an important production of pro-inflammatory cytokines and chemokines, including TNFα, CCL5, CXCL1 and CXCL10 (**Fig. 2N and S5**).

Collectively, these findings demonstrate that CAR-M can enhance distal T cell activation not through antigen cross-presentation, but by creating a pro-inflammatory cytokine milieu, thereby promoting adaptive immune responses.

CAR-M–tumor interactions result in phagocytic and non-phagocytic outcomes

As the presence of tumor cells is required in our model for CAR-M to adopt a pro-inflammatory phenotype, we next sought to dissect early CAR-M tumor cell interactions and determine how these interactions shape CAR-M effector functions. To this end, we quantified phagocytosing macrophages in co-cultures of CAR-M with different CD19-expressing tumor cell types (**Fig. 3A**). Tumor cells were engineered to express a dual-fluorescent phagocytosis reporter (**Fig. 3A)**, which exploits the differential pH sensitivity of CFP and YFP: live tumor cells are YFP^{high} at steady state (magenta), whereas internalization and degradation within the acidic phagolysosomal compartment result in progressive loss of YFP fluorescence (YFP^{low}, blue) (22). Phagocytosing macrophages were defined as $F4/80^+$ CAR-bearing macrophages exhibiting low YFP expression. Unexpectedly, although the proportion of phagocytosing macrophages varied across tumor types, phagocytic CAR-M accounted for no more than 35% of the CAR-M population over 1 h (**Fig. 3B**). To further clarify CAR-M–tumor interaction dynamics, we next performed real-time imaging *in vitro* (**Fig. 3C and Movie S1**). This analysis revealed two distinct outcomes following CAR-M engagement with tumor cells. Only 40% of CAR-M quickly engulfed tumor cells (**Fig. 3D**) reinforcing our previous flow cytometry data.

Importantly, these results cannot be accounted solely to the level of CAR expression as more than 95% of all CAR-M expressed CAR MFI as high as the phagocytic population (YFP^{low}) (**Fig.S7**). Interestingly, phagocytosis occurred after a short median contact time of 6 min following tumor addition, further suggesting that CAR-M are intrinsically "poised" to phagocytosis (**Fig. 3E-F and S6**). Interestingly, live imaging also revealed that a substantial fraction of CAR-M established prolonged and stable contacts with tumor cells without phagocytosing them, and this was also true in other tumor models of different origins (Eμ-Myc, **Fig. 3C, 3E-H, movies S1-2** and MC38, **Fig. S6 and movie S2**). Importantly, a subset of CAR-M maintained stable contacts with tumor cells for up to 280 min without subsequent engulfment, defining a population of non-phagocytic CAR-M (**Fig. 3G-H and movie S3**). Together, these results indicate that both phagocytic and non-phagocytic interaction outcomes are intrinsic and coexisting features of CAR-M–tumor cell engagement which cannot solely be explained by different CAR levels.

Tumor engagement by non-phagocytic CAR-M triggers intracellular calcium signaling.

To determine whether non-phagocytic CAR-M–tumor interactions elicit intracellular signaling capable of promoting CAR-M effector functions, we analyzed calcium (Ca^{2+}) flux, an early signaling event associated with macrophage activation during phagocytosis (23). CAR-M and control macrophages were engineered to express the Förster resonance energy transfer (FRET)–based Ca^{2+} sensor Twitch2B ($Twitch2B^{CAR\text{-}M}$ and $Twitch2B^{Empty}$, respectively), allowing real-time monitoring of intracellular Ca^{2+} dynamics by time-lapse imaging (**Fig. 4A**) (24). As expected, phagocytic $Twitch2B^{CAR\text{-}M}$ exhibited one or multiple transient Ca^{2+} fluxes upon tumor contact, followed by target engulfment (**Fig. 4B and Movie S4**). Notably, Ca^{2+} signals were also observed in $Twitch2B^{CAR\text{-}M}$ establishing stable contacts with tumor cells in the absence of phagocytosis, indicating that non-phagocytic CAR engagement is sufficient to trigger intracellular signaling. By contrast, control $Twitch2B^{Empty}$ failed to exhibit detectable Ca^{2+} fluxes, underscoring the requirement for CAR expression in signal induction (**Fig. 4B-C and movies S4-S6**). Together, these results demonstrate that CAR-M–tumor cell interactions induce CAR-dependent Ca^{2+} signaling irrespective of phagocytosis occurrence, providing direct evidence that non-phagocytic CAR engagement initiates intracellular signaling events that may contribute to CAR-M effector functions.

Although a significant fraction of CAR-M fails to phagocytose tumor cells, whether these non-phagocytic interactions contribute to the overall CAR-M efficacy remained unclear. To dissociate the impact of CAR signaling from those of phagocytosis, we developed an experimental approach to induce CAR engagement independently of target engulfment. Twitch 2B-expressing CAR-M were imaged in real time while CAR molecules were crosslinked using a CD19-based complex consisting of a CD19-Fc chimeric protein and a secondary anti-Fc Fab fragment (**Fig. 4D**). Under these conditions, $Twitch2B^{CAR\text{-}M}$ displayed a transient Ca^{2+} flux that was absent in control $Twitch2B^{Empty}$, demonstrating that Ca^{2+} signaling occurs specifically through CD19-mediated CAR crosslinking even in the absence of phagocytosis (**Fig. 4E-F and movies S7-8**). This approach, therefore provides a tool to model non-phagocytic CAR engagement.

CAR signaling, regardless of target engulfment, is sufficient to induce a pro-inflammatory CAR-M phenotype.

To determine whether non-phagocytic CAR-M signaling is sufficient to induce CAR-M effector programs, we performed an unbiased bulk RNA sequencing analysis comparing transcriptional responses induced by phagocytic and crosslinked CAR-M shortly after CAR engagement (**Fig. 5A**). To avoid contamination by engulfed tumor-derived RNA, CAR-M were co-cultured with human Daudi tumor cells engineered to express mouse CD19 and the phagocytosis reporter. Given that target engulfment induces rapid (< 1 h) transcriptional reprogramming in macrophages (25), phagocytic CAR-M (YFP^{low}) were flow-sorted after 1 h and compared to CD19-crosslinked CAR-M. As expected, phagocytosis induced extensive transcriptional remodeling at this early time point (**Fig. S8**). Strikingly, CAR signaling in the absence of phagocytosis triggered a transcriptional program that largely overlapped with that observed in phagocytic CAR-M (**Fig. 5B-C** and **S8**). Early CAR engagement led

to the upregulation of NFκB–associated pathways, as well as cytokine and chemokine transcripts, including signatures related to TNFα and inflammasome activation (**Fig. 5C**). These results indicate that CAR signaling alone is sufficient to rapidly induce a pro-inflammatory transcriptional program in CAR-M, independently of target engulfment.

We next asked whether these early transcriptional changes translated into functional effector responses. To this end, we performed multiplex ELISA analyses to quantify cytokines and chemokines produced by CAR-M cultured either in contact with tumor cells or stimulated with the CD19 crosslinking complex. TNFα and CXCL1 were also detected in the supernatants under both conditions, along with additional chemokines including CCL5 and CXCL10 (**Fig. 5D**). Thus, CAR signaling in the absence of phagocytosis drives robust production of pro-inflammatory mediators, just like CAR-mediated phagocytosis.

Finally, we investigated whether soluble factors produced upon CAR crosslinking were sufficient to enhance T cell activation. Using a transwell system, CTV-labelled naïve OT-I cells were co-cultured with tumor cells and physically separated from CAR-M either engaging tumor cells or stimulated with the CD19 complex (**Fig. 5E**). Under these conditions, CAR crosslinking alone was sufficient to enhance naïve T cell activation, to a degree comparable to that observed with phagocytosing CAR-M (**Fig. 5F**). Collectively, these data demonstrate that CAR signaling, independently of phagocytosis, is sufficient to induce a pro-inflammatory CAR-M phenotype and promote T cell activation, establishing non-phagocytic CAR engagement as a functional and therapeutically relevant mode of CAR-M action.

DISCUSSION

Here, we extend previous work showing that CAR-M can enhance antitumor T cell responses and show that, in our model, this effect is primarily driven by CAR-dependent cytokine and chemokine production. To delineate the cellular mechanisms underlying this activity, we relied on real-time imaging to dissect early CAR-M–tumor cell interactions. This approach revealed pronounced functional heterogeneity within the CAR-M population, with a substantial fraction of CAR-M failing to phagocytose tumor cells. Despite the lack of target engulfment, non-phagocytic CAR-M established sustained contacts with tumor cells that were sufficient to (1) trigger CAR-dependent Ca^{2+} signaling, (2) induce a pro-inflammatory transcriptional and functional program, and (3) ultimately promote T cell activation and proliferation. Together, these findings support a model in which CAR signaling in non-phagocytic CAR-M represents a previously underappreciated contributor to overall CAR-M effector function.

In this study, we have combined real time imaging with tumor cells expressing a fluorescent pH-sensitive phagocytosis reporter to investigate early CAR-M and tumor cells interactions. Consistent with previous reports, we observed marked heterogeneity in phagocytic efficiency across tumor types, both *in vitro* and *in vivo*. In our experimental system, phagocytosis efficacy ranged from 10% to up to 40% of all CAR-M, depending on tumor model, with lower rates observed for B16 melanoma cells and higher rates for B cell-derived tumors. Heterogeneity in macrophage-mediated phagocytosis has been proposed to be directly influenced by target intrinsic properties, including size and cellular phenotype. Although these parameters were not directly quantified here, they are likely to contribute to our observed differences. Indeed, ProB and Eμ-Myc tumor cells, which exhibited the greatest proportion of CAR-M-mediated engulfment, are of B cell origin and comparatively smaller in size than B16 melanoma tumor cells, which are of stromal origin. In addition, phenotypic differences between these tumor types may further tune phagocytosis efficacy. Interestingly, similar tumor-intrinsic heterogeneity is likely to exist in the clinical setting, where tumor cells vary widely across cancer types and patients (26). Together, these findings suggest that tumor-intrinsic features substantially influence CAR-M phagocytic outcomes and contribute to the functional heterogeneity observed within the CAR-M population.

Beyond target-dependent effects, our study also describes substantial heterogeneity within the CAR-M population itself. Characterization of phagocytosis dynamics revealed a short median engulfment time of 6 min. This suggests a pre-existing intrinsic capacity for CAR-M to engulf tumor cells rather than a sole reliance on CAR engagement, a feature that appears heterogeneous at the level of the CAR-M population. Some studies have proposed that macrophages origin or cell shape could be a determinant for their phagocytic capacity (27, 28). In our system, macrophage size does not seem to correlate with phagocytic behavior in our live imaging analyses, indicating that alternative intrinsic determinants likely underlie this functional diversity. One possibility is lineage-related heterogeneity among bone marrow-derived progenitors, which may give rise to macrophage subsets with distinct phagocytic competencies and contribute to the observed variability within the CAR-M population.

Previous studies have reported that CAR-M can mediate trogocytosis (29), a process involving partial membrane transfer from target cells that may induce tumor cell stress and apoptosis (30, 31). It would be interesting to further evaluate whether stable CAR-M-tumor contacts result in trogocytosis, a phenomenon that we could not observe in our set-up due to cytoplasm-localized fluorescent tumor probe. Thus, while our data emphasize full phagocytosis and sustained contact-dependent signaling, we cannot exclude a potential contribution of trogocytosis under alternative experimental conditions.

Functionally, we show that CAR-M reduce tumor burden at early time points, both *in vitro* and *in vivo*. However, sustained tumor control at later stages requires an intact adaptive immune system, as highlighted with prior reports demonstrating the importance of CAR-M–T cell crosstalk for durable antitumor efficacy (19, 20). While prior studies have linked CAR-M–driven T cell activation to antigen cross-presentation, our data indicate that, in our model, T cell enhancement is largely mediated by CAR-dependent cytokines and chemokines. Differences in the inflammatory state of CAR-M across studies may contribute to these divergent observations. Supporting antigen presentation-independent mechanisms, MHC class I–deficient CAR-M retained partial antitumor activity (20), further implicating cytokine-mediated pathways in CAR-M-driven adaptive immune responses.

Collectively, our study identifies CAR-driven inflammatory signaling, including in non-phagocytic macrophages, as a critical component of their antitumor function. These findings have important implications for designing next-generation CAR-M therapies and strengthen the rationale for incorporating signaling components that engage proinflammatory signaling pathways. In line with this concept, recent studies have shown that third-generation CAR activating TLR4 intracellular signaling pathways can induce tumor cell apoptosis and CAR-M-mediated efferocytosis. This leads to enhanced survival in preclinical models (32). Such strategy targeting cytokine signalization would also enable a bystander mode of action, facilitating the elimination of antigen-negative tumor cells that would not be engulfed if CAR-M solely relied on phagocytosis. Whether such CAR engineering strategy can be extended to other cytokine pathways remains to be explored.

Ultimately, this study positions CAR engagement, regardless of target engulfment, as a key contributor of CAR-M overall mode of action, that endows macrophages with T cell activating functions, opening new avenues to improve CAR-M therapeutic design.

MATERIAL AND METHODS

Mice. Five-to-twelve-week-old female and male C57BL/6J were purchased from Envigo. *Rag2*-deficient mice, Ubi^{GFP}-OT-I, OT-I *Rag2*$^{-/-}$ and Ly5.1^{+}*Rag2*$^{-/-}$ under a C57BL/6 background were bred in our animal facility under specific-pathogen-free conditions, air renewal, ambient temperature of 22 ± 2 °C and controlled light–dark cycle. All experiments were approved by Institut Pasteur's Safety Committee in accordance with French and European guidelines (CETEA 220108, CETEA 240110, CETEA 230038).

Plasmids. All used plasmids were subcloned into a MSCV backbone. The CAR plasmid encodes a chimeric antigen receptor composed of an extracellular single chain variable fragment (scFv) targeting mouse CD19, a CD8 transmembrane domain, and an intracellular domain containing the FcR-γ immunoreceptor tyrosine-based activation motif (ITAM) and the p85-recruiting motif of murine CD19 (17). The CAR^{CTRL} plasmid encodes a chimeric antigen receptor only comprising the extracellular scFv targeting mouse CD19 and transmembrane domain, lacking any intracellular signaling motives (33). Furthermore, plasmids encoding the probes DEVD (34) and Twitch2B (24), gifted by Oliver Griesbeck, were used. The cytoplasmic ovalbumin (OVA) encoding plasmid was gifted by Maria Castro (35).

Cell lines. The leukemic ProB cell line (36) and the lymphoma myc-over expressing cell line (Eμ-myc mice (37)) were retrovirally transduced to express a fluorescent-based phagocytosis reporter probe (named here DEVD) (22). Human B cell Daudi tumors (ATCC, CCL-213) were retrovirally transduced to express the DEVD phagocytosis reporter as well as murine CD19 and CD20 molecules. All B cell tumor models were cultured in RPMI-1640 (Gibco) supplemented with 10% heat-inactivated fetal bovine serum (Sigma), 50 U.mL^{-1} penicillin (Gibco), 50 µg.mL^{-1} streptomycin (Gibco), 1 mM sodium pyruvate (Gibco), 10 mM HEPES (Gibco), and 50 µM 2-mercaptoethanol (Gibco) (complete RPMI). The melanoma cell line B16_F10 (ATCC) was retrovirally transduced to express the DEVD probe as well as the murine CD19 protein (38). HEK293T (ATCC) and L929 (ATCC) and the generated B16-DEVD-CD19 were cultured in DMEM (Gibco) supplemented with 10% heat-inactivated fetal bovine serum (Sigma), 50 U.mL^{-1} penicillin (Gibco), 50 µg.mL^{-1} streptomycin (Gibco), 1 mM sodium pyruvate (Gibco), 10 mM HEPES (Gibco), and 50 µM 2-mercaptoethanol (Gibco) (complete DMEM). The colon carcinoma cell line MC38 (Kerafast) was modified to express the DEVD probe as well as murine CD19 protein (38). When indicated, the cells were further genetically modified to express the cytosolic ovalbumin protein. Cells were cultured in DMEM (Gibco) supplemented with supplemented with 10% heat-inactivated fetal bovine serum (Sigma), 50 U.mL^{-1} penicillin (Gibco), 50 µg.mL^{-1} streptomycin (Gibco), 1 mM sodium pyruvate (Gibco), 10 mM HEPES (Gibco), 50 µM gentamicin (Sigma) and 1mM non-essential amino acids (Sigma). All cell lines were cultured at 37°C, 5% CO_2 and regularly tested for mycoplasma contamination (Minerva Biolabs).

Generation of β2m-deficient tumor cell lines. DEVD^{+} CD19^{+} OVA^{+} β2m-deficient MC38 tumor cells were generated from the parental line MC38 DEVD^{+} CD19^{+}OVA $^{+}$ using the genotype editing Alt-RTM CRISPR-Cas9 System (Integrated DNA Technologies) and following manufacturer's recommendations. The sequences used to target β2m was CACGCCACCCACCGGAGAAT. Effective β2m ablation was confirmed by flow cytometry.

Generation of bone-marrow derived macrophages (BMDMs). Bone-marrow derived macrophages were generated as described previously (39). Briefly, bone-marrow was extracted from C57BL/6J and cultured for at least 6 days with 20% L929 supernatant in complete RPMI. Transduced macrophages were generated by two rounds of spin-infections (performed at 4 and 24 h). In case of double transduction, viral particles encoding each one plasmid were mixed at a 1:1 ratio. After the second spin-infection, the cells were detached and plated in non-tissue-culture treated 15 cm dishes with complete medium supplemented with 20% L929 supernatant. Once the cells were differentiated, the

macrophages were detached using cold 1X PBS followed by a 15 min incubation with cell dissociation buffer (PBS supplemented with 5 mM EDTA) at 4°C.The transduction rate (around 50-80%) of the cells was screened by flow cytometry using cell surface expression of human CD34 reporter. Unless specified otherwise, macrophages were always kept in complete medium supplemented with 20% L929 supernatant.

Purification of CAR-M. CAR^{CTRL}-M or CAR-M were purified according to their CAR expression as defined by cell surface expression of human CD34 protein using hCD34-positive selection following the manufacturer's instructions (Miltenyi). Purification efficiency (>70%) was screened by flow cytometry.

CD19 crosslinking complex. To generate the CD19 complex, the murine CD19-Fc chimera (R&D Biosystems) was incubated with anti-Fc Fab (Jackson Immunoresearch Laboratories) at a ratio of 1:2 for at least 10 min before addition to the cells for a final concentration of 2.5 $\mu g.mL^{-1}$ of CD19-Fc and 5 $\mu g.mL^{-1}$ anti-Fc Fab.

***In vitro* phagocytosis analysis.** Untransduced BMDM, CAR^{CTRL}-M or CAR-M were plated. On the day of the assay, tumor cells (Eμ-Myc, ProB, MC38 or B16_F10) were added to the macrophages at an effector:target ratio of 1:1 for 1 h. The supernatant of the wells was removed, the cells washed with cold PBS and incubated for 15 min at 4°C with cell dissociation buffer (Gibco) to allow detachment by pipette flushing.

Real-time phagocytosis dynamic imaging. Untransduced macrophages or CAR-M were plated at a concentration of 10^6/well cells in 6 cm dishes for at least 24 h before imaging. Imaging was performed as described previously (39). Briefly, on the day of imaging, the macrophages were stained using anti-F4/80-Alexa594 (clone BM8, Biolegend) in PBS supplemented with 0.05% FCS for 20 min at room temperature in the dark. The staining solution was removed and replaced with imaging medium (RPMI lacking phenol red (Gibco) supplemented with 5% FCS). Macrophages were imaged at steady-state before addition of 10^6 cells Eμ-Myc $DEVD^+$ or MC38 $DEVD^+CD19^+$ tumors. Acquisition was then performed for at least 2 h. *In vitro* imaging was performed with an upright microscope (FVMPE-RS, Olympus), a 25×/1.05 numerical aperture, water-dipping objective combined with an objective heater and using FV31S-SW software (Olympus). Excitation was provided by an Insight DeepSee dual laser (Spectra-Physics) tuned at 830 nm. The following filters were used for fluorescence detection: DEVD (CFP:483/32, YFP: 542/27), A594 (593/40). Acquisition was also performed on the upright Stellaris Dive microscope (Leica), a 25×/1.05 numerical aperture, water-dipping objective combined with an objective heater (Olympus) and using the Leica Application Suite X (v 4.5.0.25531, Leica). Excitation was provided by a Coherent Vision II laser (BD Biosciences) tuned at 830 nm. The following detection settings were used: CFP (449-505 nm), YFP (530-550 nm), A594 (560-600 nm) and background (620-650 nm). To create time-lapse sequences, we typically scanned a 20 μm-thick volume at 4 μm Z-steps and 1 min intervals.

Real-time imaging of calcium signaling. Bone-marrow derived macrophages transduced with the retrovirus encoding the Twitch2B probe ($Twitch2B^{Empty}$) or the CAR-encoding retrovirus and the Twitch2B probe ($Twitch2B^{CAR\text{-}M}$). Imaging was performed as described above: macrophages were imaged for 30 min at steady-state before the addition of 10^6 cells Eμ-Myc tumor cells stained with 5μM SNARF dye (Invitrogen). Acquisition was then continued for at least 1h. In parallel, macrophages were imaged for 15-20 min at steady state before the addition of the complexed CD19 antigen. Acquisition was then continued for at least 30 min. Acquisition was performed on the upright Stellaris Dive microscope (Leica), a 25×/1.05 numerical aperture, water-dipping objective combined with an objective heater (Olympus) and using the Leica Application Suite X (v 4.5.0.25531, Leica). Excitation was provided by a Coherent Vision II laser (BD Biosciences) tuned at 880 nm. The following detection settings were used: SNARF (637-665 nm), SNARF (571-604 nm), calcium high (536-558 nm), calcium

low (468-515 nm). To create time-lapse sequences, we typically scanned a 16 µm-thick volume at 4 µm Z-steps and 20s intervals.

Real-time imaging analysis. Movies were processed and analyzed using Fiji software (Version 2.14.0/1.54f). Figures and videos based on two-photon microscopy are two-dimensional maximum or average intensity projections of three-dimensional data. CAR-M-tumor interactions were quantified manually. A prolonged interaction is defined as any interaction lasting at least 1 min. Phagocytosis was defined as the moment the tumor cell was fully surrounded by macrophage cell membrane.
Calcium signaling was quantified using Fiji (2.14.0/1.54f). Briefly, macrophages of interest were contoured and median fluorescence intensity in the calcium high and calcium low channels were extracted for each frame. The ratio of calcium high/calcium low was then computed and normalized to the first frame of the movie.

Mixed-species bulk RNAseq analysis. Empty or CAR-M were plated at $2x10^6$ cells/well in 6-well untreated cell culture plates. On the day of the experiment, either Daudi-DEVD-CD19 tumors were added at an effector:target ratio of 2:1, or the CD19 antigen complex was added before 1 h of incubation. Cells were then detached as previously described and filtered on 70 µm filters. The single-cell suspension was stained in a Fc-blocked flow cytometry buffer (2% FBS, 0.2% EDTA in PBS) containing anti-CD16/32 antibody (BioLegend) for 20 min at 4°C with the monoclonal antibodies: anti-human CD34 Alexa 647 (clone 561, Biolegend) and anti-F4/80 BV711 (clone BM8, Biolegend). Phagocytosing macrophages were sorted by gating on high CAR-expressing macrophages and then on the YFP^{low} population. Sorting was performed on FACS Aria III (BD Biosciences) using a 100 µm nozzle. Cells were collected in FCS supplemented with 1 mM EDTA (Gibco). RNA extraction was then performed using the RNAeasy extraction kit (Qiagen). RNA concentrations were measured on the Qubit (Invitrogen) and a quality control performed on the TapeStation (Agilent). mRNA libraries were generated and sequenced at the internal platform (Biomics) using the Index Dual RNA kit (IDT). Libraries were sequenced on the Illumina NovaSeq 2000 (100bp, single-end, 100M reads per sample). Raw data quality was assessed and reports generated using FastQC v.0.12.1 and gathered using multiqc v1.25. We performed a 3 steps mapping: sequencing reads were first mapped to the pMSCV-CARmacro-1D3-tandem-hCD34 using BWA-MEM v0.7.19-r1273. The unmapped reads were recovered using samtools v1.21. These reads were mapped to human genome GRCh38 downloaded from ensembl 112 using STAR v2.7.10b. Then the reads not mapped on the human genome were mapped to the mouse genome GRCm39 downloaded from ensembl 112. After mapping, we used feature Counts from Subread (version 2.0.6) to generate the gene-level count matrix. We performed the matrix normalization and differential gene expression analyses by the package DESeq2 v 1.50 in R 4.5.0. Differentially expressed genes were defined as genes with a false discovery rate (FDR) ≤ 0.05 and |Log2FC| ≥ 0.584. Plots were generated using R Studio (v2024.12.1+563).

Multiplex assays for cytokine quantification. M^{UTD}, M^{Empty}, CAR^{CTRL} or CAR-M macrophages were plated in the presence or absence of Eµ-Myc tumors at an effector: target ratio of 1:1 for 24 h. For the crosslinking condition, the CD19-antigen complex was added to CAR-M for 24 h at 37°C. M^{UTD} were also incubated with 1 µm mL^{-1} LPS (Sigma) for 24 h. At the end of the assay, the supernatant was collected from the cells and spun down at 300g for 5 min to remove any cellular debris. Multiplex cytokine assay was performed using a custom 17-Plex ProcartaPlex Panel (Invitrogen). Plates were incubated overnight at 4°C under agitation and analyses were performed using a Bio-Plex 200 system and the Bio-Plex Manager software (Bio-Rad). Data are represented as a z-score calculated using this formula: $z = \frac{x - \mu}{\sigma}$ where x is the value of interest, µ the average of all the values of the sample and σ the standard-deviation of all values of the samples.

CAR-M T cell co-culture assay. Naïve OT-I $CD8^+$ T cells were isolated from (Ubi^{GFP})-OT-1 TCR-*Rag1*$^{-/-}$ transgenic mice, labeled with the Cell Trace Violet (CTV) Proliferation Dye (Thermo Fisher Scientific) according to the manufacturer's instructions. Untransduced or CAR-bearing macrophages and MC38-$DEVD^+$-$CD19^+$-OVA^+ or MC38-$DEVD^+$-$CD19^+$-OVA^+-$\beta2m^{-/-}$ tumors were co-cultured in an

effector: target ratio of 5:1. After 4 h of co-culture, the tumors were washed by flushing with PBS (Gibco). Then the stained naïve OT-I T cells were added at a T cell: macrophage ratio of 5:1 in the presence of 10 ng mL^{-1} human IL-2 (R&D Systems).

Transwell assays. 0.5 M control macrophages (M^{UTD} or M^{Empty}), CAR^{CTRL}-M or CAR-M were plated at the bottom of 24-well transwell bearing plates (Corning). On the day of the experiment, MC38-$DEVD^{+}$-$CD19^{+}$-OVA^{+} tumor cells were added at an effector: target ratio of 5:1 to the macrophages. 4 h later, the tumor cells were washed with PBS. 10^4 MC38-$DEVD^{+}$-$CD19^{+}$-OVA^{+} were added to the top of transwell with 0.8 x10^6 naïve OT-I T cells, generated as described above to mimic the tumor microenvironment and antigen presence. For the cross-linking condition, no tumor cells were added to the macrophages but the CD19-antigen complex at a final concentration of 2.5 µg.mL^{-1} of complex. All conditions were incubated for 72 h in the presence of 10 ng.mL^{-1} human IL-2 (R&D Systems). In the last 4 h, GolgiPlugTM (BD Biosciences) was added to the culture according to manufacturer's instructions.

***Ex vivo* analysis of the antitumoral activity of CAR-M.** C57BL/6 female or male mice of 6-12 weeks were injected i.p. with 4M ProB-DEVD (male tumor) or 5M MC38-$DEVD^{+}$-$CD19^{+}$-OVA^{+} (female) tumors respectively 48 or 24 h before treatment with PBS, untransduced, empty or CAR-bearing macrophages differentiated from *Rag2*$^{-/-}$ x Ly5.1 mice bone-marrow as described above using complete RPMI medium supplemented with 20 ng.mL^{-1} m-CSF (Peprotech). 1 or 2 days post-treatment, a peritoneal lavage was performed. The collected cells were then spun down and resuspended in red blood cell lysis buffer (Invitrogen) for 5 min. After addition of PBS, the suspension was filtered on 70 µm filters, resuspended and stained.

Flow cytometry. All flow cytometry staining were done in flow cytometry buffer (2% FBS, 0.2% EDTA in PBS) with anti-CD16/32 antibody (BioLegend), mice serum (1:50), unless otherwise specified.

<u>Antibody mix for CAR-M transduction efficacy:</u> Cells were stained with fixable viability dye eF780 (Invitrogen) for 20 min using following monoclonal antibodies: anti-human CD34 A647 (clone 561, Biolegend), anti-human CD34 PE (clone 561, Biolegend), anti-F4/80 BUV395 clone BM8, eBiosciences), anti-Ly6C BV786 (clone HK1.4, Biolegend), anti-G4S Linker A647 (clone E702V, Cell Signalling).

<u>Antibody mix for phagocytosis assays</u>: Cells were stained with fixable viability dye eF780 (Invitrogen) for 20 min using following monoclonal antibodies: anti-IA/IE BUV395 (clone M5/114.15.2, BD Biosciences), anti-F4/80 BV711 (clone BM8, Biolegend), anti-human CD34 PE (clone 561, Biolegend), anti-CD86 PE-Cy7 (clone GL-1, Biolegend), anti-CD64 APC (clone X54-5/7.1, Biolegend).

<u>Antibody mix for CAR-M and T cell co-culture:</u> Cells were stained with fixable viability dye eF780 (Invitrogen) for 20 min using following monoclonal antibodies: anti-IA/IE BUV737 (clone M5/114.15.2, BD Biosciences), anti-PDL1 BUV395 (clone MIH5, BD Biosciences), anti-F4/80 PE-Cy7 (clone BM8, Biolegend), anti-CD45.2 BV605 (clone 104, Biolegend), anti-CD40 A647 (clone HM40-3, BD Biosciences), anti-human CD34 PE (clone 561, Biolegend), anti-CD86 BV650 (clone GL-1, Biolegend), anti-TCRβ BUV395 (clone 53-6.7, BD Biosciences), anti-F4/80 BV711 (clone BM8, Biolegend), anti-PD-1 (clone RMP1-14, Biolegend), anti-CD69 APC (clone H1.2F3, Biolegend).

<u>Antibody mix for transwell assay</u>: Cells were stained with fixable viability dye eF780 (Invitrogen) for 20 min using following monoclonal antibodies: Anti-CD8 BUV395 (53-6.7, BD Biosciences), anti-CD44 BV605 (clone IM7, Biolegend), anti-F480 BV711 (clone BM8, Biolegend), anti-CD25 A488 (clone PC61, Biolegend), anti-PD-1 PE-Cy7 (clone RMP1-14, Biolegend), anti-CD62L APC (clone MEL-14, Biolegend), anti-CD8 PE-Cy7 (clone 53-6.7 , Biolegend) and anti-F4/80 APC-Cy7 (clone BM8, Biolegend). For intracellular protein staining, the samples were fixed and stained using the CytoFix

CytoPerm kit according to manufacturer's instruction (BD Biosciences). The following antibodies were used: Anti-IFNγ BUV737 (clone XMG1.2, BD Biosciences), anti-TNFα A488 (clone MP6-XT22, Biolegend), anti-Granzyme B PE (clone QA18A28, Biolegend), anti-Perforin APC (clone S16009B, Biolegend).

Antibody mix for *in vivo* analysis of tumor load: Single cell suspension obtained as described above were stained with fixable viability dye eF780 (Invitrogen) for 20 min using following monoclonal antibodies: Anti-CD19 BUV395 (clone 1D3, BD Biosciences), anti-CD45.2 BUV737 (clone 104, BD Biosciences), anti-B220 BV786 (clone RA3-6B2, Biolegend), anti-NK1.1 PE (clone PK136, Biolegend), anti-human CD34 (clone 561, Biolegend), anti-CD45.1 PE-Cy7 (clone A20, Biolegend), anti-CD8 A647 (clone 53-6.7, Biolegend), anti-TCRβ BV421 (clone 53-6.7, Biolegend), anti-CD45.1 PE (clone A20, Biolegend) anti-F4/80 PE-Cy7 (clone BM8, Biolegend) anti-B220 APC (clone RA3-6B2, Biolegend), anti-human CD34 A700 (clone 581, Biolegend), anti-TCRβ APC-Cy7 (clone 53-6.7, Biolegend), anti-Ly6G BUV395 (clone 1A8, BD Biosciences), anti-Ly6C BV786 (clone HK1.4, Biolegend), anti-CD19 BV421 (clone 6D5, Biolegend), anti-CD11b PerCP5.5 (clone M1/70, Biolegend), anti-CD64 APC (clone X54-5/7.1, Biolegend).

For evaluation of absolute counts of cells, counting beads (AccuCheck or 123count, ThermoFisher) were added before acquisition on the LSR Fortessa (BD Biosciences) or Cytoflex (Beckman-Coulter). All flow cytometry data was analyzed using FlowJo v10.

Proliferation analysis. T cell proliferation was analyzed using the Proliferation analysis tool of Flowjo v10. The division index is defined as the average number of divisions for all cell culture calculated as such: $DI = \frac{\sum_0^i i \times \frac{N_i}{2^i}}{\sum_0^i \frac{N_i}{2^i}}$ where i is the generation number and N^i the number of events in generation i.

Statistical analysis. All statistical tests were performed with Prism v.10.6.1 (GraphPad). Data are expressed as mean ± SEM. We used t-tests for two-group comparison and one-way or two-way analysis of variance (ANOVA) for multiple comparison. All statistical tests were two-tailed with a significance level of 0.05. *P < 0.05, **P < 0.01, ***P < 0.001; ns, non-significant.

ACKNOWLEDGMENTS

We thank all members of the Bousso laboratory for support and helpful discussions. Particularly, we thank Nicolas Serafini for critical review of this study. We would like to thank Sébastien Lemoine and Emeline Perthame for their advice about bulk RNAseq analysis. We would also like to thank Ophélie Godon and Friederike Jonsson for sharing reagents and technical input. At the Institut Pasteur, we acknowledge the Central Animal Facility, in particular animal caretakers for their daily help, the CBUTechS platform for cytometry support, and the BIOMICS platform for the Bulk RNA Seq experiment, especially Yakov Vitrenko and Laure Lemée Biomics Platform, C2RT, Institut Pasteur, Paris, France, supported by France Génomique (ANR-10-INBS-09) and IBISA. This work is supported by grants from Institut Pasteur (P.B, L.F.), Institut National de la Santé et de la Recherche Médicale (Inserm, P.B, C.LG), European Research Council (ENLIGHTEN, P.B), La Ligue contre le Cancer (P.B), ANR JC/JC (C.L.G) and a Ph.D funding from Studienstiftung des deutschen Volkes (Promotionsstipendium, L.F.) and La Fondation ARC (ARCDOC42024120009175, L.F).

AUTHOR CONTRIBUTIONS

According to the CrediT taxonomy (40). Conceptualization: C.L.G.; Methodology: L.F., A.V., F.L., B.C., Z.G., C.L.G.; Investigation: L.F., C.V., R.A., B.C., C.L.G.; Data curation: L.F., A.V.; Formal analysis: L.F., A.V., Visualization: L.F., C.L.G, ; Writing – original draft: L.F., M.V.G., C.L.G.; Writing – review & editing: L.F., F.L., C.V., R.A., B.C., M.V.G., C.L.G.; Resources: P.B.; Supervision: P.B., M.V.G, C.L.G.; Project administration: C.L.G.; Funding acquisition: P.B., C.L.G.

DECLARATION OF INTERESTS

The authors declare that they have no competing interests.

MATERIALS AND CORRESPONDENCE

All data needed to evaluate the conclusions are present in the paper and the supplementary materials. Further information for the study should be directed to and will be fulfilled by the corresponding author C.L.G., upon reasonable request.

FIGURE LEGEND

Figure 1. CAR-M generated by retroviral transduction are not pro-inflammatory at steady state and reduce tumor load *in vitro* and *in vivo*.

A. Schematic representation of the chimeric antigen receptor (CAR) expressed in macrophages. The CAR comprises an extracellular single-chain variable fragment (scFv) targeting mouse CD19, a CD8 transmembrane domain, and an intracellular domain containing the FcR-γ immunoreceptor tyrosine-based activation motif (ITAM) and the p85-recruiting motif of murine CD19. **B.** Experimental scheme of the transduction protocol. Murine bone marrow cells were isolated, retrovirally transduced twice (day 0 and day 1), and differentiated into macrophages using L929 supernatant or m-CSF. **C–D.** Experimental design (C) and multiplex ELISA quantification of cytokines and chemokines (D) produced by untransduced macrophages (M^{UTD}), sham-transduced (M^{Empty}), or CAR-expressing macrophages (CAR-M), compared with LPS-stimulated untransduced macrophages. Supernatants were collected at 24 h post-stimulation and are represented as a z-score (n = 3-11 biological replicates). **E–G.** Experimental scheme (E), representative contour plots of the live cells after 24 h (Eμ-Myc) and tumor load quantification (G) following co-culture of CAR-M or control macrophages with CD19-expressing tumor cells, including two B cell tumor models (ProB and Eμ-Myc; 24 h) and solid tumors (MC38 colon carcinoma and B16_F10 melanoma; 48 h). Tumor load was measured by flow cytometry and normalized to control tumor wells alone (n = 5–6 independent biological replicates; statistical analysis by t-tests). **H-I.** Experimental scheme (G) and tumor load (H) 24 h (ProB) or 48 h (MC38) after i.p. injection of CAR-M or control macrophages (M^{UTD} or M^{Empty}) into ProB or MC38-bearing C57BL/6 mice. Tumor load was measured by flow cytometry and normalized to the control condition (n = 7–9 mice from 2 independent experiments; statistical analysis by unpaired t-test). Error bars represent mean ± SEM. ***P < 0.001; **P < 0.01; *P < 0.05. See Methods for additional experimental details.

Figure 2. CAR-M–mediated enhancement of antigen-specific CD8$^+$ T cell activation. **A–B.** Schematic representation of the experimental set-up (A) in which macrophages (M^{UTD} or CAR-M) were co-cultured with WT CD19$^+$ OVA$^+$ MC38 or *β2m*-deficient tumor cells for 4 h at an effector-to-target (E:T) ratio of 5:1. Tumor cells were subsequently washed before the addition of naïve CTV-labelled OT-I T cells at a CAR-M:T cell ratio of 5:1 and cultured in presence of IL-2 for a total of 72 h. OT-I T cell proliferation was assessed by flow cytometry and quantified using the division index (B) (n = 3–5 independent biological replicates from 5 independent experiments. Statistical analysis by ratio-paired t-test). **C-F**. Schematic of the transwell experimental set-up (C) in which macrophages (CAR^{CTRL}-M, or CAR-M) and CD19$^+$ OVA$^+$ MC38 tumor cells were plated in the lower chamber, while naïve OT-I T cells and OVA$^+$ CD19$^+$ MC38 tumor cells were placed in the upper chamber of the transwell assay. T cells were analysed by flow cytometry after 72 h in presence of IL-2, as shown in representative flow cytometry profiles (D). Quantification of the T cell division index (E) and the proportion of activated CD25$^+$ T cells (F) are shown. (n = 5 independent experiments, statistical analysis by ratio paired t-test). **G.–I.** Granzyme B expression by OT-I. G. Representative histograms of the expression of Granzyme B. Quantification of the expression levels of Granzyme B following the transwell assay, shown as mean fluorescence intensity (MFI) normalized to CAR^{CTRL}-M (H) and as percentage of positive of OT-I (I) cells (n = 5 independent experiments, statistical by ratio unpaired t-test (H) or ratio-paired t-test (I)). **J.** Proportion of TNFα^{high} OT-I T cells following the transwell assay (n = 5 independent experiments; statistical analysis by ratio-paired t-test). **K–L**. Representative flow cytometry profiles (K) and quantification (L) of CD44 and CD62L expression on activated OT-I T cells following the transwell assay with CAR-M or CAR^{CTRL}-M (n = 5 independent experiment, statistical analysis by ratio-paired t-test). **M-N.** Experimental scheme (M) and multiplex ELISA quantification of cytokines and chemokines (N) produced when CAR^{CTRL} transduced macrophages (CAR^{CTRL}-M) or CAR-expressing macrophages (CAR-M) were co-cultured with tumor cells (Eμ-Myc). Data are shown as a z-score and are from n = 3-11 independent experiments. Supernatants were collected at 24 h post-stimulation. Error bars represent mean ± SEM. ***P < 0.001; **P < 0.01; *P < 0.05. See Methods for additional experimental details.

Figure 3. CAR-M tumor interactions result in phagocytic and non-phagocytic outcomes.
A-B. Experimental scheme (A) of a 1h co-culture of CAR-M with CD19-expressing tumor cells expressing a probe for phagocytosis. Schematic representation of tumor cells expressing the fluorescence phagocytosis probe. At a physiological level, tumor cells express both the CFP and YFP fluorescence (magenta). Upon phagocytosis, YFP fluorescence is gradually lost as tumor cells are engulfed into the highly acidic environment of the phagolysosome, appearing blue during live imaging Quantification (B) of phagocytic CAR-M was carried out as the proportion of F4/80$^+$ CAR-bearing (CAR^{CTRL}-M and CAR-M) or not (M^{UTD}) YFP^{low} cells in different tumor models (n = 3-7 independent experiments, statistical analysis by paired one-way ANOVA or paired t-test). **C**. Representative time-lapse imaging of the dynamics of CAR-M (green) in co-culture with Eμ-Myc tumors expressing the fluorescence probe. Live tumors appear magenta, engulfed tumor cells are blue. Stable contacts are encircles while an arrow points to the phagocytosis (representative of 3 independent experiments; scale bar, 20 μm). **D.** Proportion of phagocytic CAR-M across all analyzed movies and imaging positions. Each point represents one analyzed position; dot shapes indicate independent experiments (n = 3 independent experiments). **E.** Movie analysis showing interaction dynamics between CAR-M with Eμ-Myc tumor cells during 2 hours of co-culture. Each line represents a CAR-M in contact with a least one tumor cell and each square a minute of acquisition. CAR-M in contact with tumor cells appear green, a phagocytosis event corresponds to a pink square (data pooled from 3 independent experiments, 67 CAR-M analyzed). **F.** Duration of tumor cell contact time preceding phagocytosis events (data pooled from 3 independent experiments, 49 phagocytosis events analyzed). **G**. Representative time-lapse imaging of the dynamics of CAR-M (green) in co-culture with Eμ-Myc tumors expressing the fluorescence probe for 4,5 hours. The arrow indicates a stable contact. Live tumors appear magenta, engulfed tumor blue (representative of 3 independent experiments; scale

bar, 20 µm). **H**. Quantification of the duration of contacts between CAR-M and Eµ-Myc tumor cells in time-lapse imaging over 284 minutes (data pooled from 3 independent experiments, 312 stable contacts were analyzed). Error bars represent mean ± SEM. ***P < 0.001; **P < 0.01; *P < 0.05. See Methods for additional experimental details.

Figure 4. Regardless of outcome, CAR-tumor interactions can trigger calcium signals.
A-C. Experimental set up (A) and representative images (B) of a co culture of tumor cells and CAR-M (top) or control macrophages expressing (bottom) a calcic probe Twitch2B (CAR-$M^{Twitch2B}$ and $Empty^{Twitch2B}$). Images were acquired every 20 s (scale bar, 10 µm). Added Eµ-Myc tumor cells appear blue (representative of 3 independent experiments). Calcium signals were collected from image analyses and are shown in (C). Prolonged contacts with tumor cells appear in green on the quantification, and phagocytosis events in magenta. **D-F.** Experimental scheme (D) and representative images (E) showing live imaging of Twitch 2B-expressing CAR-M or Twitch-2B macrophages ($Twitch2B^{Empty}$) during addition of the CD19-crosslinking complex. Images are representative of 3 independent experiments and were acquired every 20 s (scale bar, 10 µm). (F) Quantification of the calcium signal in $Twitch2B^{CAR-M}$ or $Twitch2B^{Empty}$ macrophages in the presence of the CD19 complex (orange).

Figure 5. CAR signalling is sufficient for CAR-M mediated-cytokine/chemokine production. **A**. Experimental scheme of the mixed-species bulk RNAseq set-up. Murine purified CAR-M were incubated for 1 h with the CD19-complex, or with human B cell tumors (Daudi) transduced to express murine CD19 and the phagocytosis probe. Control CAR-M did not receive any treatment. Phagocytic CAR-M were identified based on their YFP^{low} fluorescence and flow cytometry sorted. All three conditions were sequenced together. Analysis was performed by first mapping the reads onto the human genome and excluding all reads mapping there, then performing the mapping on the murine genome. The experiment included 3-5 biological replicates and was performed independently twice. **B.** Scatterplot representing the mean expression of each gene in the CAR phagocytosing condition (x-axis) compared to the CAR crosslinking condition (y-axis). **C**. Heatmap representing the relative expression of genes associated to pro-inflammatory pathways that are significantly differentially regulated in phagocytic or crosslinked CAR-M (n = 3-5 independent experiments). **D.** Absolute concentration of CXCL1, CXCL10, CCL5 and TNFα measured in co-culture of control macrophages (M^{Empty}) or CAR-M with Eµ-Myc tumor cells for 24 h. CAR-M were also cultured in the presence of the CD19 complex for 24 h (CAR crosslinking) (n= 3 independent replicates, statistical analysis was performed by paired one-way ANOVA). **E-F**. Schematic experimental set-up (E) showing the transwell assay. Macrophages (Control (M^{UTD} or M^{Empty}) or CAR-M) and tumor cells were plated at the bottom part while naïve CTV-stained OT-I T cells were added with MC38-OVA on the upper part of the well. For the crosslinking condition, CAR-M were left without tumor cells at the bottom and the CD19 complex was added for 24 h. 72 h later T cell proliferation was measured by CTV dilution by flow cytometry and graphed in (F) (n = 4 independent experiments, statistical analysis was performed by paired one-way ANOVA). Error bars represent mean ± SEM. ***P < 0.001; **P < 0.01; *P < 0.05. See Methods for additional experimental details.

SUPPLEMENTARY FIGURE LEGEND

Figure S1. Generation and characterization of CAR-M.

A. Experimental scheme of the transduction protocol of CAR-M using retroviral infection. **B.** Representative dot plot of the expression of F4/80 and Ly6C by CAR-M after 6 days of differentiation *in vitro*. **C.** Representative histogram of the transduction level of M^{UTD} or CAR-M measured by the level of hCD34 expression after purification of the CAR-M. Representative of more than 10 independent experiments. **D.** Representative contour plot of the expression of the CAR on M^{UTD} (grey) or CAR-M (blue) as measured by hCD34 expression versus a direct CAR-staining using the anti-linker antibody.

Figure S2. Absolute concentrations in the supernatant of M^{UTD}, M^{Empty} or CAR-M at steady-state of different cytokines and chemokines.

Supernatants were collected at 24 h post-stimulation (n = 3-11 independent experiments, statistical analysis by one-way ANOVA). Error bars represent mean ± SEM. See Methods for additional experimental details. ***$P < 0.001$; **$P < 0.01$; *$P < 0.05$

Figure S3. *β2m*$^{-/-}$ tumor controls and T cell proliferation flow cytometry profile.

A. Representative histograms of the expression levels of MHC-I (H2kB staining) of WT, *β2m*-deficient or unstained tumour cells. **B.** Representative histograms of the proliferation profile (CTV) of naïve OT-I T cells in presence of M^{UTD} or CAR-M primed with WT or *β2m*-deficient tumor (n = 3-5 independent experiments).

Figure S4. Granzyme B profile and absolute T cell counts in CAR^{CTRL}-M and CAR M.

A. Absolute count of OT-I T cells in transwell assays in presence of CAR^{CTRL}-M or CAR-M. Counts were normalized to the CAR^{CTRL}-M condition (n = 5 independent experiments, statistical analysis by unpaired t-test). **B.** Representative expression of Granzyme B and CTV of naïve OT-I T cells (black), OT-I T cells T cells in presence of CAR^{CTRL}-M (turquoise) or CAR-M (blue) (representative of 5 independent experiments). **C.** Representative expression of TNFα and CTV of naïve OT-I T cells (black), OT-I T cells T cells in presence of CAR^{CTRL}-M (turquoise) or CAR-M (blue) (representative of 5 independent experiments).

Figure S5. Normalized concentrations of cytokines and chemokines in the supernatant of CAR^{CTRL}-M or CAR-M in presence of Eμ-Myc tumor cells.

Supernatants were collected at 24 h post-stimulation and cytokine/chemokine concentrations normalized to the condition in absence of tumor cells (n = 3-11 independent experiments, statistical analysis by paired t-test). Error bars represent mean ± SEM. ***$P < 0.001$; **$P < 0.01$; *$P < 0.05$ See Methods for additional experimental details.

Figure S6. Phagocytosis dynamics for MC38 tumor cells.

A. Representation of the interaction dynamics of CAR-M with MC38 tumor cells during 2 h of co-culture. Each line represents a CAR-M in contact with a least one tumor cell, each square a minute of acquisition. CAR-M in contact with tumor cells appear green, a phagocytosis event pink (data pooled from 3 independent experiments, 158 CAR-M analyzed). **B**. Phagocytosis events depending on the contact time between CAR-M and MC38 tumor cells before phagocytosis (data pooled from 3 independent experiments, total of 69 phagocytosis events analyzed).

Figure S7. CAR level expression on phagocytosing CAR-M.

CAR expression (hCD34 expression) of total CAR-M population or phagocytosing CAR-M (YFP^{low}). Histogram representative of 5 independent experiments.

Figure S8. Mixed-species bulk RNAseq analysis

A. Schematic representation of the analysis pipeline of the mixed-species bulk RNAseq data. Percentages indicate the remaining non excluded reads at each step. **B.** Volcano plot representing the differentially expressed genes in the CAR crosslinking condition to CAR-M at steady-state. **C.** Volcano plot representing the differentially expressed genes in the phagocytosing CAR-M condition to CAR-M at steady-state (n = 3 -5 biological replicates, from 2 independent experiments).

Legends and description of the supplementary movies

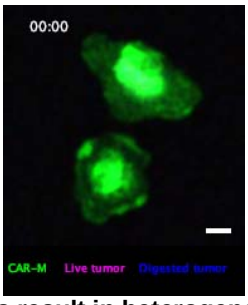

Movie S1 – CAR-M tumor interactions result in heterogeneous outcomes.
Representative time-lapse imaging of the dynamics of CAR-M (green) in co-culture with Eμ-Myc tumors expressing the fluorescence reporter of phagocytosis. Live tumors appear magenta, engulfed tumor cells are blue (representative of 3 independent experiments; scale bar, 10 μm, time is indicated in minutes).

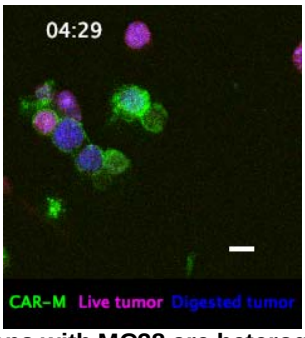

Movie S2 – CAR-M tumor interactions with MC38 are heterogeneous.
Representative time-lapse imaging of the dynamics of CAR-M (green) in co-culture with MC38 CD19^{+} tumors expressing the fluorescence reporter of phagocytosis. Live tumors appear magenta, engulfed tumor cells are blue (representative of 3 independent experiments; scale bar, 10 μm, time is indicated in minutes).

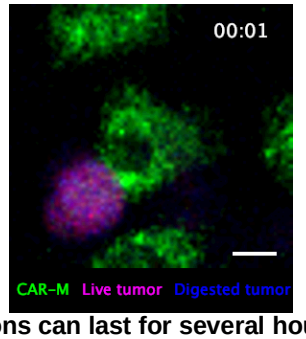

Movie S3 – CAR-M tumor interactions can last for several hours.
Representative time-lapse imaging of the dynamics of CAR-M (green) in co-culture with Eμ-Myc tumors expressing the fluorescence reporter of phagocytosis for 4,5 hours. Live tumors appear magenta, engulfed tumor would appear blue (representative of 3 independent experiments; scale bar, 10 μm, time is indicated in minutes).

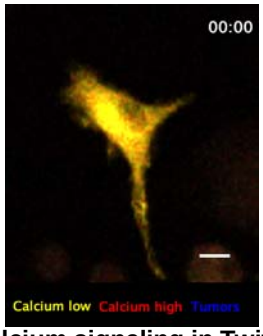

Movie S4 – Phagocytosis induces calcium signaling in Twitch2B-expressing CAR-M.
Representative time-lapse imaging of a Twitch-2B expressing CAR-M (yellow-red) in co-culture with Eμ-Myc tumor cells (blue). Intracellular calcium increase appears red. (scale bar, 10 μm, representative of 3 independent experiments, time is indicated in seconds).

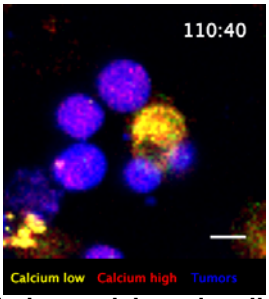

Movie S5 – Prolonged contacts can induce calcium signaling in Twitch2B-expressing CAR-M.
Representative time-lapse imaging of a Twitch-2B expressing CAR-M (yellow-red) in co-culture with Eμ-Myc tumor cells (blue). Intracellular calcium increase appears red. (scale bar, 10 μm, representative of 3 independent experiments, time is indicated in seconds).

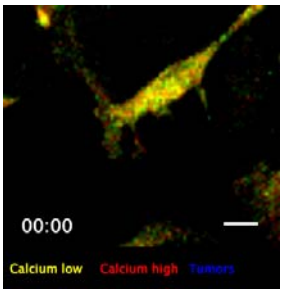

Movie S6 – Prolonged contacts do not induce calcium signaling in control macrophages.
Representative time-lapse imaging of a Twitch-2B expressing macrophage (yellow-red) in co-culture with Eμ-Myc tumor cells (blue). Intracellular calcium increase appears red. (scale bar, 10 μm, representative of 3 independent experiments, time is indicated in seconds).

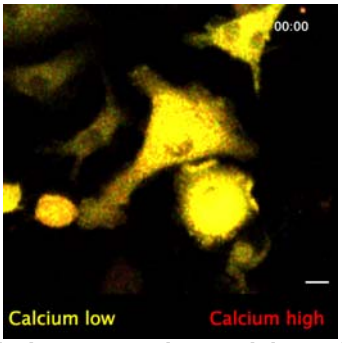

Movie S7 – The CD19 complex induces transient calcium signaling in Twitch2B-expressing CAR-M.
Representative time-lapse imaging of a Twitch-2B expressing CAR-macrophage (yellow-red) before and after addition of the CD19 complex. Intracellular calcium increase appears red. (scale bar, 10 µm, representative of 3 independent experiments, time is indicated in seconds).

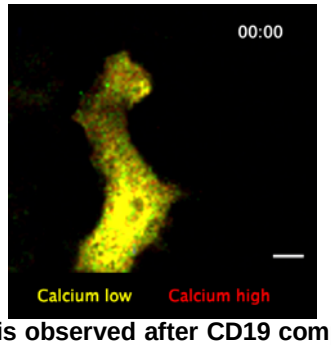

Movie S8 – No calcium signaling is observed after CD19 complex addition to a control Twitch-2B expressing macrophage.
Representative time-lapse imaging of a Twitch-2B expressing macrophage (yellow-red) before and after addition of the CD19 complex. Intracellular calcium increase appears red. (scale bar, 10 µm, representative of 3 independent experiments, time is indicated in seconds).

REFERENCES

1. D. G. DeNardo, B. Ruffell, Macrophages as regulators of tumor immunity and immunotherapy. *Nat Rev Immunol* **19**, 369–382 (2019).

2. D. J. Kloosterman, L. Akkari, Macrophages at the interface of the co-evolving cancer ecosystem. *Cell* **0** (2023).

3. A. Mantovani, P. Allavena, F. Marchesi, C. Garlanda, Macrophages as tools and targets in cancer therapy. *Nat Rev Drug Discov* **21**, 799–820 (2022).

4. M. D. Park, *et al.*, TREM2 macrophages drive NK cell paucity and dysfunction in lung cancer. *Nat Immunol* **24**, 792–801 (2023).

5. M. J. Pittet, O. Michielin, D. Migliorini, Clinical relevance of tumour-associated macrophages. *Nat Rev Clin Oncol* **19**, 402–421 (2022).

6. M. A. Cannarile, *et al.*, Colony-stimulating factor 1 receptor (CSF1R) inhibitors in cancer therapy. *J Immunother Cancer* **5**, 53 (2017).

7. C. H. Ries, *et al.*, Targeting tumor-associated macrophages with anti-CSF-1R antibody reveals a strategy for cancer therapy. *Cancer Cell* **25**, 846–859 (2014).

8. G. L. Beatty, *et al.*, CD40 Agonists Alter Tumor Stroma and Show Efficacy Against Pancreatic Carcinoma in Mice and Humans. *Science* **331**, 1612–1616 (2011).

9. S. M. McWhirter, C. A. Jefferies, Nucleic Acid Sensors as Therapeutic Targets for Human Disease. *Immunity* **53**, 78–97 (2020).

10. M. Seiffert, *et al.*, Human signal-regulatory protein is expressed on normal, but not on subsets of leukemic myeloid cells and mediates cellular adhesion involving its counterreceptor CD47. *Blood* **94**, 3633–3643 (1999).

11. D. Tseng, *et al.*, Anti-CD47 antibody–mediated phagocytosis of cancer by macrophages primes an effective antitumor T-cell response. *Proceedings of the National Academy of Sciences* **110**, 11103–11108 (2013).

12. M. P. Chao, *et al.*, Anti-CD47 Antibody Synergizes with Rituximab to Promote Phagocytosis and Eradicate Non-Hodgkin Lymphoma. *Cell* **142**, 699–713 (2010).

13. S. B. Willingham, *et al.*, The CD47-signal regulatory protein alpha (SIRPa) interaction is a therapeutic target for human solid tumors. *Proc Natl Acad Sci U S A* **109**, 6662–6667 (2012).

14. S. L. Maude, *et al.*, Chimeric Antigen Receptor T Cells for Sustained Remissions in Leukemia. *New England Journal of Medicine* **371**, 1507–1517 (2014).

15. C. M. Snyder, S. I. Gill, Good CARMA: Turning bad tumor-resident myeloid cells good with chimeric antigen receptor macrophages. *Immunological Reviews* **320**, 236–249 (2023).

16. K. A. Reiss, *et al.*, CAR-macrophage therapy for HER2-overexpressing advanced solid tumors: a phase 1 trial. *Nat Med* **31**, 1171–1182 (2025).

17. M. A. Morrissey, *et al.*, Chimeric antigen receptors that trigger phagocytosis. *eLife* **7**, e36688 (2018).

18. M. Klichinsky, *et al.*, Human chimeric antigen receptor macrophages for cancer immunotherapy. *Nat Biotechnol* **38**, 947–953 (2020).

19. S. Pierini, *et al.*, Chimeric antigen receptor macrophages (CAR-M) sensitize HER2+ solid tumors to PD1 blockade in pre-clinical models. *Nat Commun* **16**, 706 (2025).

20. S. Chen, *et al.*, CAR macrophages with built-In CD47 blocker combat tumor antigen heterogeneity and activate T cells via cross-presentation. *Nat Commun* **16**, 4069 (2025).

21. C. A. Klebanoff, H. T. Khong, P. A. Antony, D. C. Palmer, N. P. Restifo, Sinks, suppressors and antigen presenters: how lymphodepletion enhances T cell-mediated tumor immunotherapy. *Trends Immunol* **26**, 111–117 (2005).

22. C. L. Grandjean, Z. Garcia, F. Lemaître, B. Bréart, P. Bousso, Imaging the mechanisms of anti-CD20 therapy in vivo uncovers spatiotemporal bottlenecks in antibody-dependent phagocytosis. *Sci Adv* **7**, eabd6167 (2021).

23. F. Nimmerjahn, J. V. Ravetch, Fcγ receptors as regulators of immune responses. *Nat Rev Immunol* **8**, 34–47 (2008).

24. T. Thestrup, *et al.*, Optimized ratiometric calcium sensors for functional in vivo imaging of neurons and T lymphocytes. *Nat Methods* **11**, 175–182 (2014).

25. T. Tufan, *et al.*, Rapid unleashing of macrophage efferocytic capacity via transcriptional pause release. *Nature* **628**, 408–415 (2024).

26. D. A. Lawson, K. Kessenbrock, R. T. Davis, N. Pervolarakis, Z. Werb, Tumour heterogeneity and metastasis at single-cell resolution. *Nat Cell Biol* **20**, 1349–1360 (2018).

27. S. Trzebanski, *et al.*, Classical monocyte ontogeny dictates their functions and fates as tissue macrophages. *Immunity* **57**, 1225-1242.e6 (2024).

28. F. Y. McWhorter, T. Wang, P. Nguyen, T. Chung, W. F. Liu, Modulation of macrophage phenotype by cell shape. *Proceedings of the National Academy of Sciences* **110**, 17253–17258 (2013).

29. K. R. Rollins, S. Fiaz, I. Datta, M. A. Morrissey, Target cell adhesion limits macrophage phagocytosis and promotes trogocytosis. *J Cell Biol* **224**, e202502034 (2025).

30. P. V. Beum, D. A. Mack, A. W. Pawluczkowycz, M. A. Lindorfer, R. P. Taylor, Binding of rituximab, trastuzumab, cetuximab, or mAb T101 to cancer cells promotes trogocytosis mediated by THP-1 cells and monocytes. *J Immunol* **181**, 8120–8132 (2008).

31. R. Velmurugan, D. K. Challa, S. Ram, R. J. Ober, E. S. Ward, Macrophage-Mediated Trogocytosis Leads to Death of Antibody-Opsonized Tumor Cells. *Mol Cancer Ther* **15**, 1879–1889 (2016).

32. A. Lei, *et al.*, A second-generation M1-polarized CAR macrophage with antitumor efficacy. *Nat Immunol* 1–15 (2023). https://doi.org/10.1038/s41590-023-01687-8.

33. M. Cazaux, *et al.*, Single-cell imaging of CAR T cell activity in vivo reveals extensive functional and anatomical heterogeneity. *Journal of Experimental Medicine* **216**, 1038–1049 (2019).

34. K. R. Garrod, *et al.*, Dissecting T Cell Contraction In Vivo Using a Genetically Encoded Reporter of Apoptosis. *Cell Reports* **2**, 1438–1447 (2012).

35. J. Yang, *et al.*, Kupfer-type immunological synapse characteristics do not predict anti-brain tumor cytolytic T-cell function in vivo. *Proc Natl Acad Sci U S A* **107**, 4716–4721 (2010).

36. H. Lenden Hasse, *et al.*, Generation and CRISPR/Cas9 editing of transformed progenitor B cells as a pseudo-physiological system to study DNA repair gene function in V(D)J recombination. *J Immunol Methods* **451**, 71–77 (2017).

37. J. M. Adams, *et al.*, The c-myc oncogene driven by immunoglobulin enhancers induces lymphoid malignancy in transgenic mice. *Nature* **318**, 533–538 (1985).

38. M. Boulch, *et al.*, Tumor-intrinsic sensitivity to the pro-apoptotic effects of IFN-γ is a major determinant of CD4+ CAR T-cell antitumor activity. *Nat Cancer* **4**, 968–983 (2023).

39. L. Feldmann, Z. Garcia, P. Bousso, C. L. Grandjean, A genetically-encoded pH-sensitive probe to image phagocytosis in real time. *In press*.

40. A. Brand, L. Allen, M. Altman, M. Hlava, J. Scott, Beyond authorship: attribution, contribution, collaboration, and credit. *Learned Publishing* **28**, 151–155 (2015).

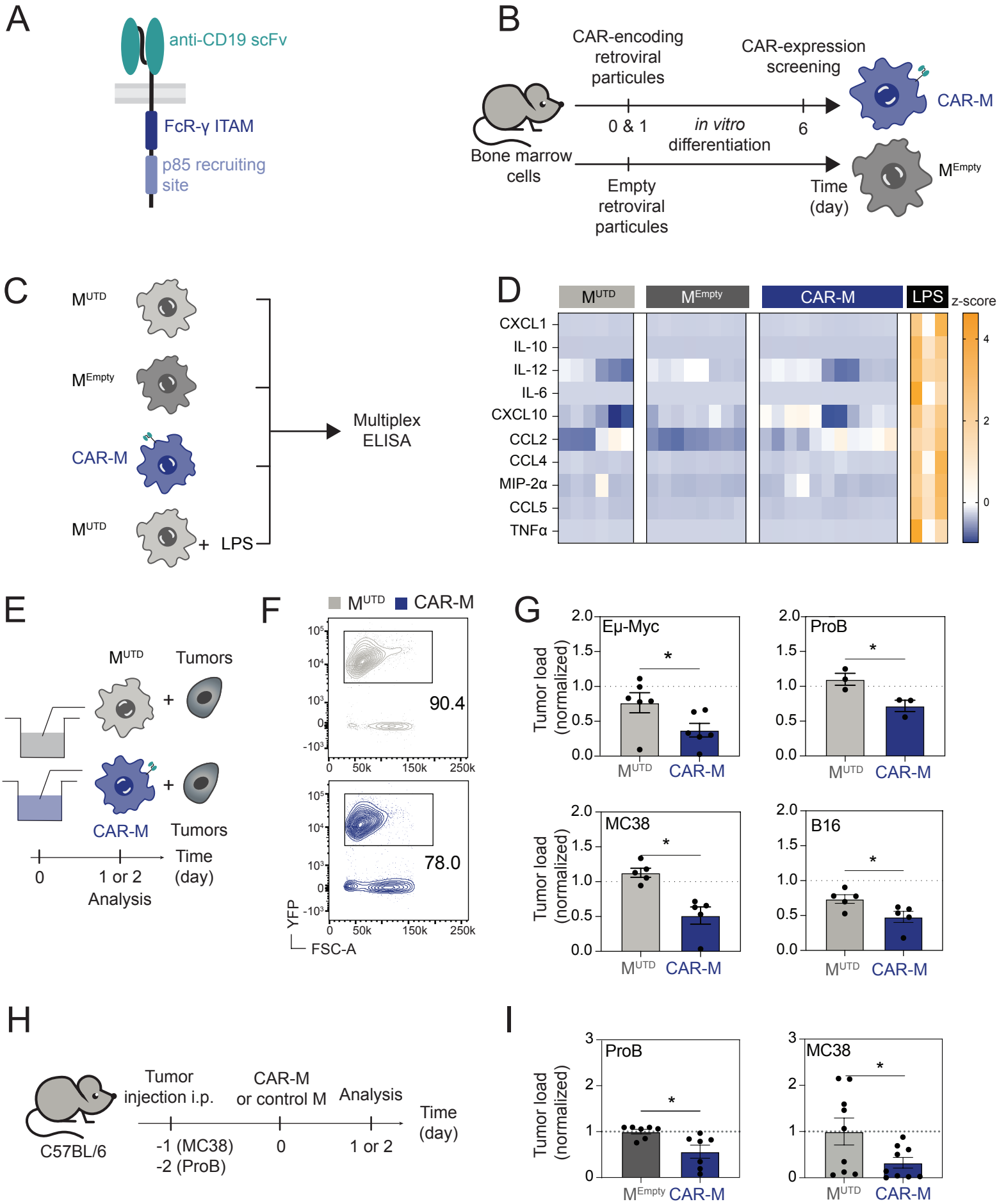

Feldmann *et al.* Figure 1

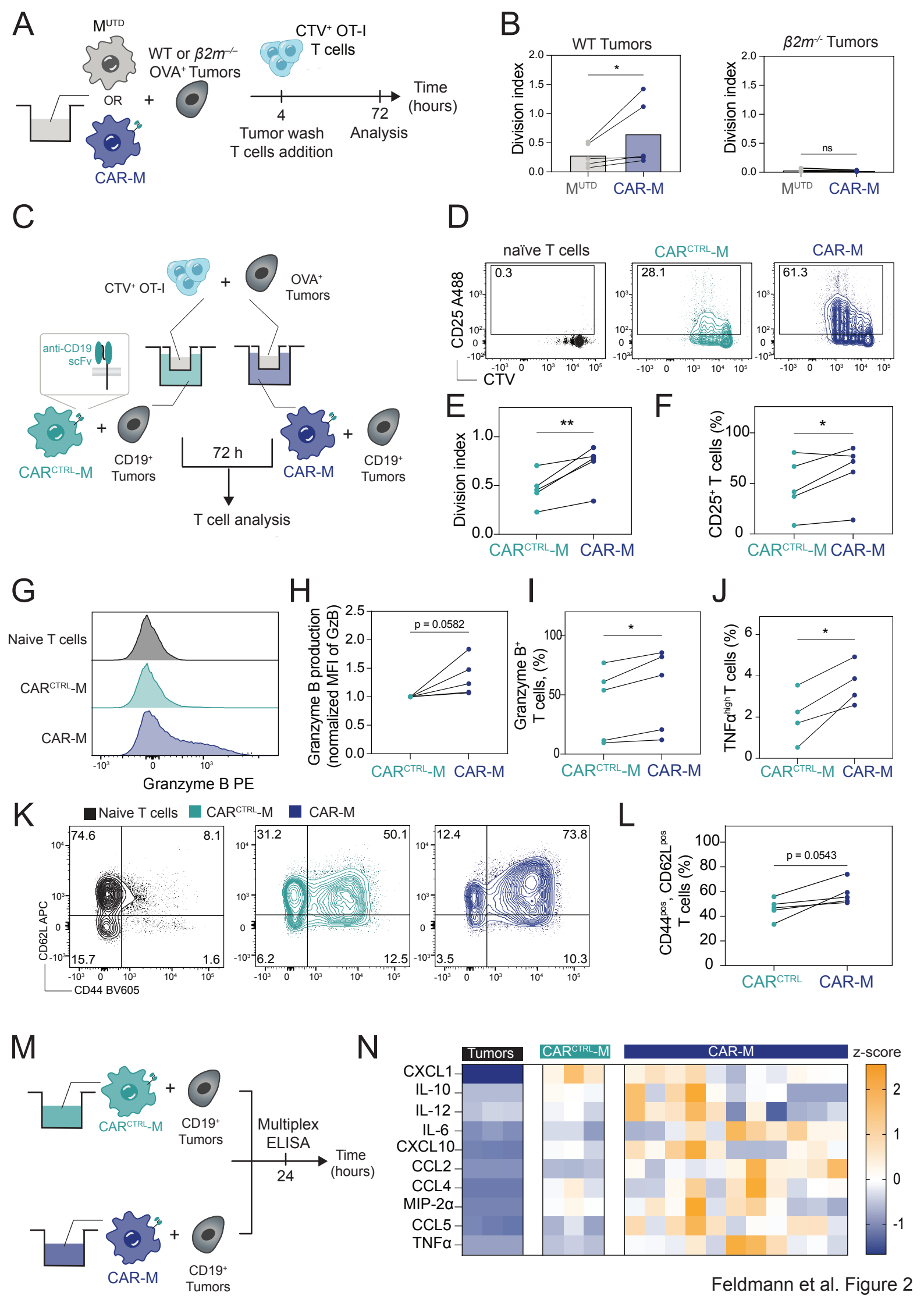

Feldmann et al. Figure 2

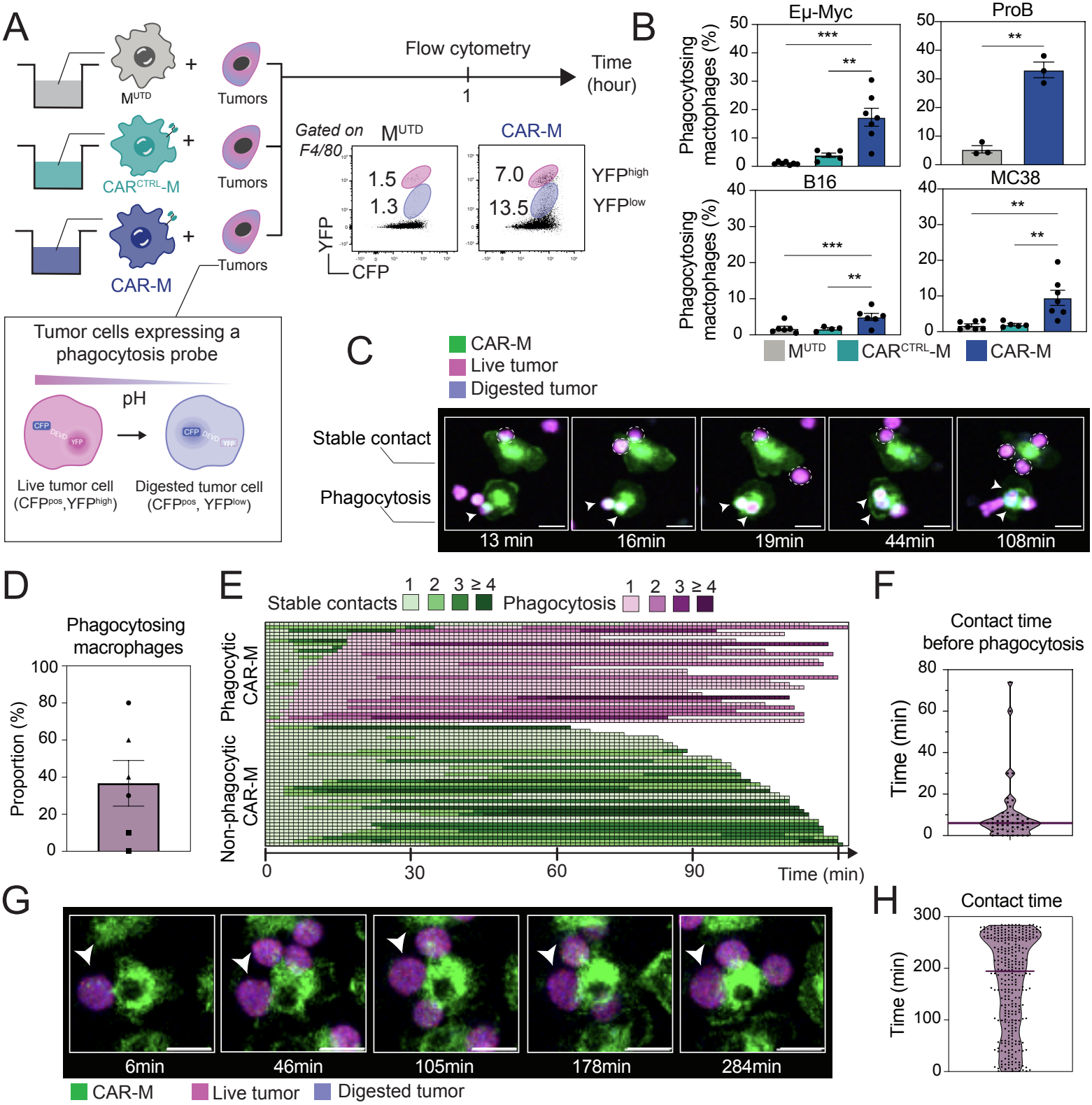

Feldmann *et al.* Figure 3

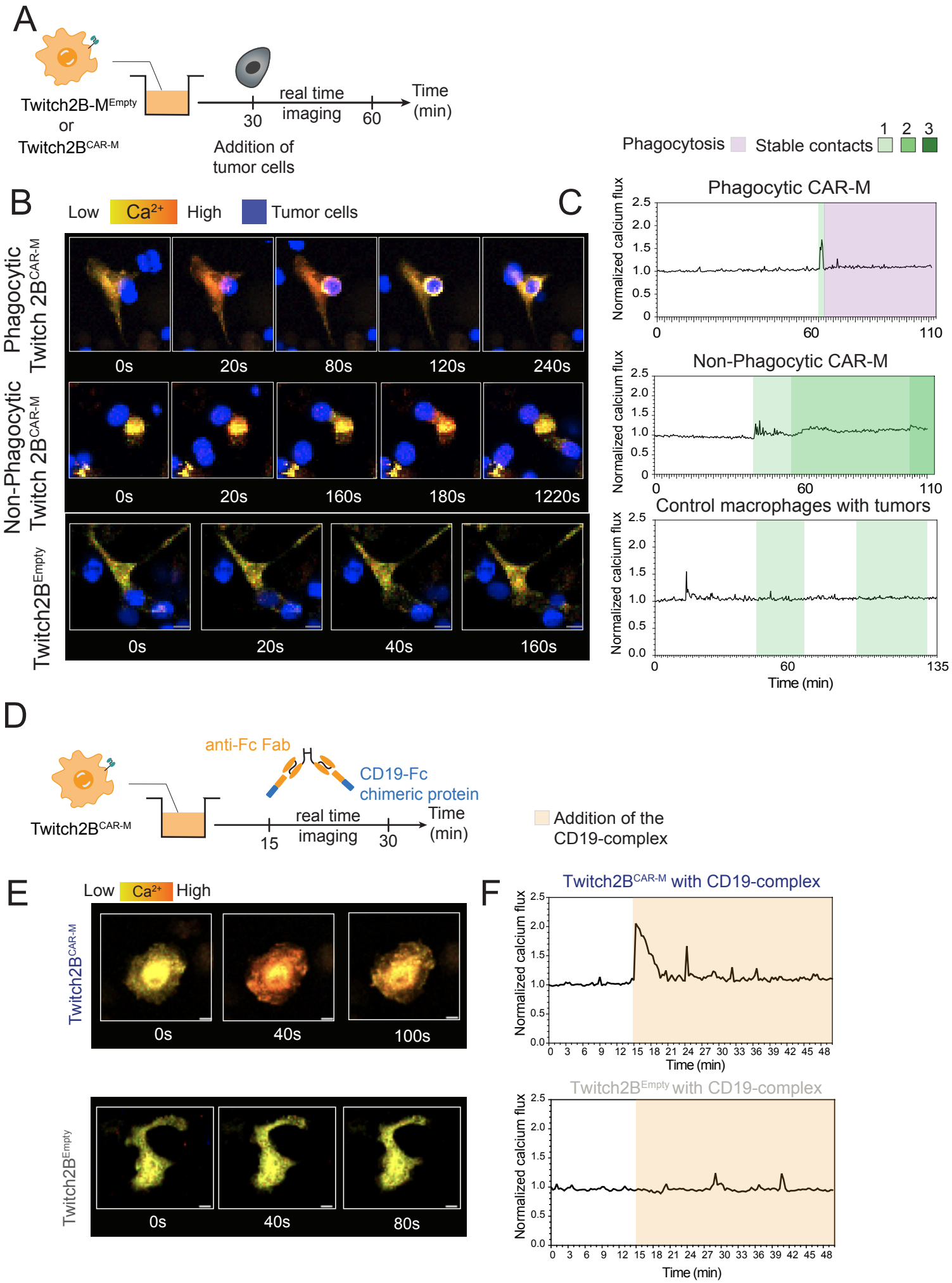

Feldmann *et al.* Figure 4

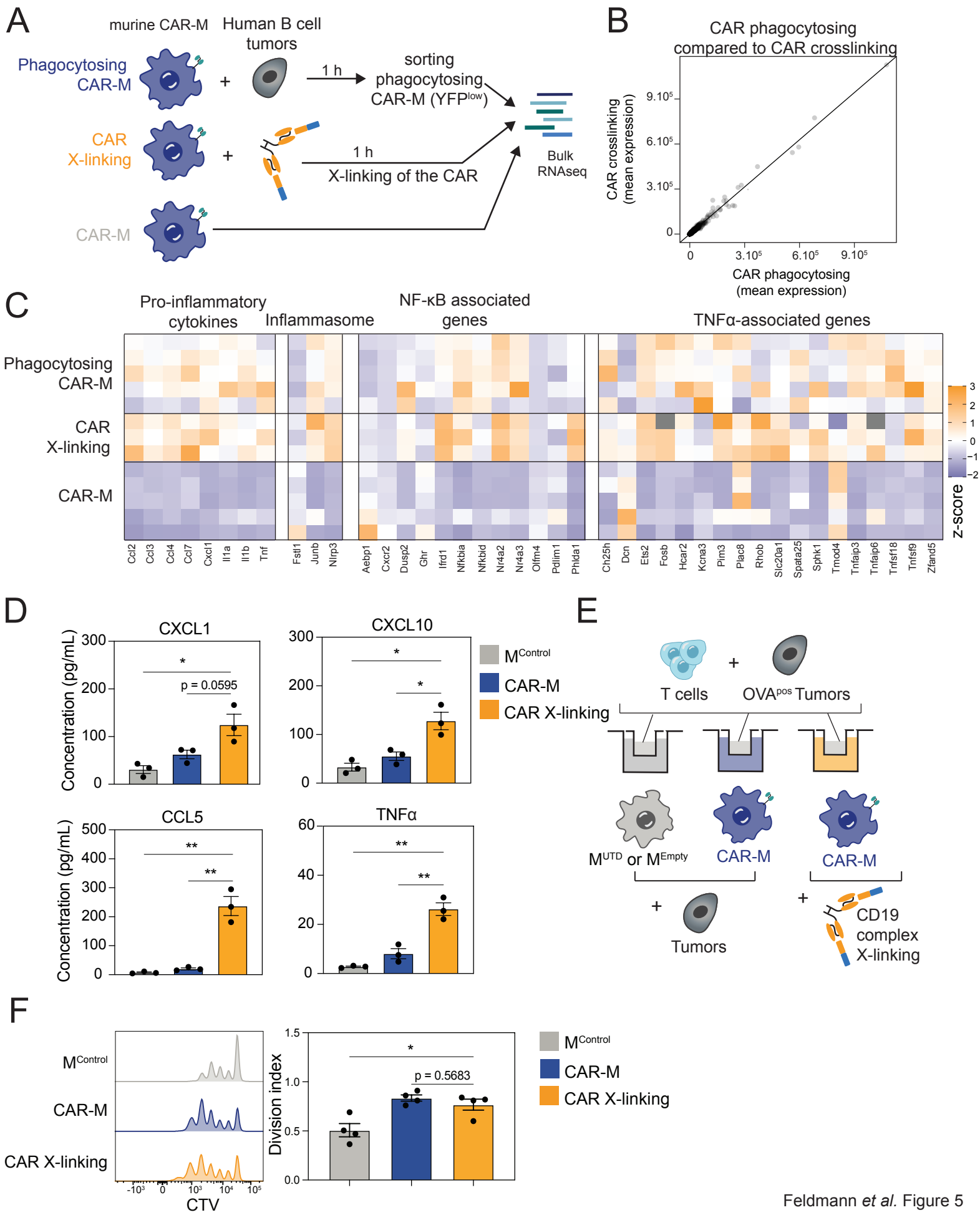

Feldmann *et al.* Figure 5